Design and Analysis of a Statically Balanced Direct-Drive Manipulator

H. Kazerooni

ABSTRACT: A statically balanced direct-drive robot has been constructed for stability analysis of the robot in constrained maneuvers. Using a four-bar linkage, a practical architecture is presented for the University of Minnesota direct-drive robot. As a result of the elimination of the gravity forces (without any counterweights), smaller actuators and, consequently, smaller amplifiers were chosen. The motors yield acceleration of five times the acceleration of gravity at the robot end point without overheating. High-torque, low-speed, brushless AC synchronous motors are used to power the robot. Graphite-epoxy composite material is used for the construction of the robot links. A four-node parallel processor has been used to control the robot. The dynamic tracking accuracy, with the feedforward torque method as a control law, has been derived experimentally. The compliance control and its stability condition have been analyzed and demonstrated experimentally.

Introduction

Direct-drive robots have two major advantages over the nondirect-drive systems. The first advantage being that the direct-drive arms are free from mechanical backlash and friction due to elimination of transmission systems. A small mechanical backlash in the transmission system would cause the gear teeth to wear faster. The high rate of wear in the gear would develop an even larger backlash. About 25 percent of the torque in nondirect-drive arms is used to overcome the friction [2]. The second advantage is such that the structural stiffness of the direct-drive arms is greater than the nondirect-drive systems. About 80 percent of the total mechanical compliance in most nondirect-drive industrial robots is caused by transmission systems [3], [4]. The high structural stiffness allows for wide-bandwidth control. The low structural stiffness of nondirect-drive arms, due to the existence of many mechanical elements in the transmission system, is a limiting factor on the achievement of a relatively wide bandwidth control system. One of the significant problems that prohibits the widespread use of existing direct-drive robots in industrial applications is their small payload in comparison with the nondirect-drive systems. The large payload of the nondirect-drive robots is due to the inherent property of the reducer transmission systems. Overheating the motors is another reported disadvantage of the nondirect-drive robots. Elimination of the transmission system causes the inertial force, and the gravitational force of the links affects the motors directly. In other words, the motors "feel" the inertial and gravitational forces without any reduction in size. The direct effect of the forces causes the motors to overheat in the direct-drive arms. This overheating exists even in the static case when the arm is only under its static load.

The work presented here is on the design and control of the Minnesota direct-drive robot [1]. This robot is statically balanced and uses a four-bar link mechanism (Fig. 1) to compensate for some of the drawbacks of the serial [5] and parallelogram [6] types of direct-drive robots. Several attempts have been made to improve the manipulator dynamic behavior. Asada and Kanade [5] designed a serial-type direct-drive arm in which the actuators were coupled directly to links without any transmission mechanism. The elimination of the transmission mechanism improved the robot's performance; however, large motors were needed to drive the robot. Asada and Youcef-Toumi [6] studied a direct-drive arm with a parallelogram mechanism to eliminate the problems associated with serial-type robots. A direct-drive arm with a counterweight was designed by Takase et al. [7] in order to eliminate the gravity effect at three major joints. Another direct-drive arm was designed by Kuwahara et al. [8] to reduce the effect of gravity using a four-bar link for the forearm and a special spring for the upper arm. The counterweight provides the system balance for all possible positions, however, it increases the total inertia of the robot arm. The spring balancing will not perfectly balance the system either [9]. In this research, a statically balanced direct-drive arm is designed to achieve improved dynamic behavior.

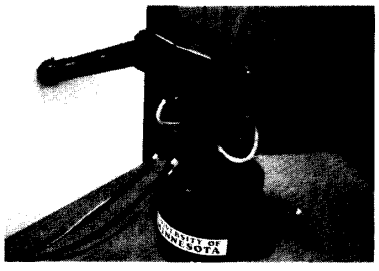

Fig. 1. University of Minnesota direct-drive robot arm.

Architecture

The architecture of this arm is such that the gravity term is eliminated completely from the dynamic equations. This balanced mechanism is designed without adding any extra counterbalance weights. The new features of this new design are as follows:

(1) Since the motors are never affected by gravity, the static load will be zero. Hence, no overheating results in the system in the quasistatic case.

(2) The elimination of gravity terms calls for smaller motors with less stall torque (and, consequently, smaller amplifiers), which have been chosen for a desired acceleration.

(3) With the lack of gravity terms, higher accuracy can be achieved. This is true because the links have steady deflection due to a constant gravity effect. This gives better accuracy and repeatability for fine manipulation tasks.

(4) The architecture of this robot allows for a "large" workspace. The horizontal workspace (radius = 80 cm) of this robot is quite attractive from the standpoint of manufacturing tasks such as assembly and deburring.

(5) Graphite-epoxy composite material is used for the construction of the robot links. This robot is lightweight (60 kg) and can be mounted on an autonomous

An earlier version of this paper was presented at the 1988 IEEE International Conference on Robotics and Automation, Philadelphia, Pennsylvania, April 24–29, 1988 [1]. H. Kazerooni is with the Mechanical Engineering Department, University of Minnesota, 111 Church Street, SE, Minneapolis, MN 55455.

0272-1708/89/0200-0030 $01.00 © 1989 IEEE

vehicle. The payload without losing precision is 2 kg.

The arm has three degrees of freedom, all of which are articulated drive joints. Motor 1 powers the system about a vertical axis. Motor 2 pitches the entire four-bar linkage, whereas motor 3 is used to power the four-bar linkage. Link 2 is connected directly to the shaft of motor 2. Figure 2 shows the top and side views of the robot. The coordinate frame $X_iY_iZ_i$ has been assigned to link i of the robot for $i = 1, 2, \ldots, 5$. The center of the coordinate frame $X_1Y_1Z_1$ corresponding to link 1 is located at point O, as shown in Fig. 2. The center of the inertial global coordinate frame $X_0Y_0Z_0$ is also located at point O. (The global coordinate frame is not shown in the figures.) The joint angles are represented by θ_1, θ_2, and θ_3, where θ_1 represents the rotation of link 1 (coordinate frame $X_1Y_1Z_1$ coincides on the global coordinate frame $X_0Y_0Z_0$ when θ_1 equals 0), θ_2 represents the pitch angle of the four-bar linkage as shown in Fig. 2, and θ_3 represents the angle between link 2 and link 3. The conditions under which the gravity terms are eliminated from the dynamic equations are shown.

Figure 3 shows the four-bar linkage with the assigned coordinate frames. By inspection, the conditions under which the vector

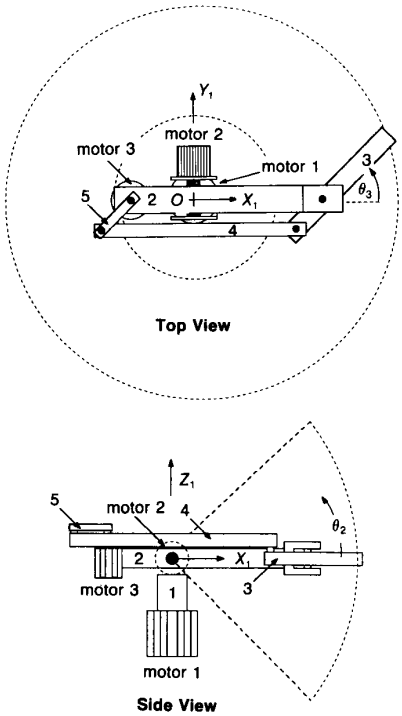

Fig. 2. Top and side views of the robot.

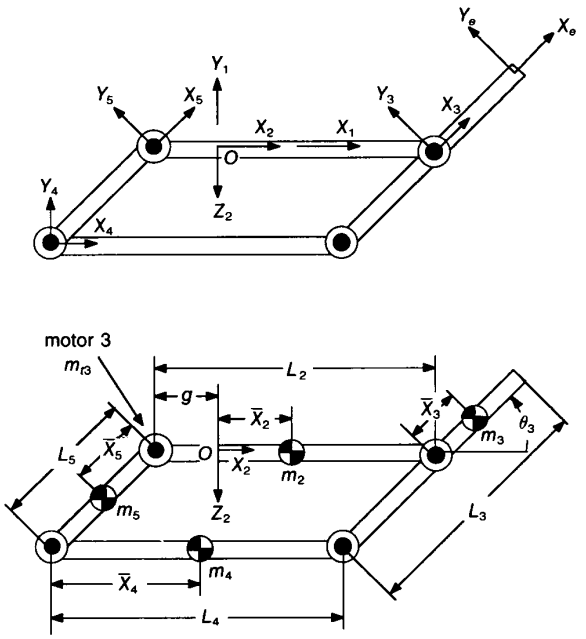

Fig. 3. Four-bar link mechanism.

of gravity passes through the origin, O, for all possible values of θ_1 and θ_3 are given by Eqs. (1) and (2). m_i, L_i are the mass and length of each link, $\bar{x}_i$ is the distance of the center of mass from the origin of each coordinate frame, and mt_3 is the mass of motor 3.

$$m_3\bar{x}_3 - m_4L_5 - m_5\bar{x}_5 = 0 \qquad (1)$$

$$g(mt_3 + m_5) - m_2\bar{x}_2 - m_3(L_2 - g) - m_4(\bar{x}_4 - g) = 0 \qquad (2)$$

If Eqs. (1) and (2) are satisfied, then the center of gravity of the four-bar linkage passes through point O for all the possible configurations of the arm. Note that the gravity force still passes through O even if the plane of the four-bar linkage is tilted by motor 2 for all values of θ_2.

Since, at low speeds, AC torque motors do not tend to cog, low-speed, high-torque, and brushless AC synchronous motors have been chosen to power the robot. Each motor consists of a ring-shaped stator and a ring-shaped permanent magnet rotor with a large number of poles. The rotor is made of rare earth magnetic material (neodymium) bonded to a low-carbon steel yoke with structural adhesive. The stator of the motor (with winding) is fixed to the housing for heat dissipation. To develop wide-bandwidth (high-speed) closed-loop control for the robot, graphite-epoxy composite and AA7075T6 materials were used to construct the links. The high structural stiffness and low density of the graphite-epoxy composite result in high natural frequencies in the robot dynamics. The higher the natural frequencies, the wider the bandwidth and, consequently, the faster the closed-loop system will be [10]. A strong bond between the composite and aluminum parts was achieved using an epoxy adhesive (3M Epoxy Adhesive EC-3569 B/A). To minimize joint clearance and reduce bearing mass, Super Precision angular contact bearings (ABEC-7, extremely light series 1900) were used.

Kinematics

The forward kinematic problem is to compute the position of the end point in the global coordinate frame $X_0Y_0Z_0$, given the joint angles θ_1, θ_2, and θ_3. The end-point position of the robot relative to the global coordinate frame is characterized by P_x, P_y, and P_z in the global coordinate

$$P_x = (C_1C_2C_3 - S_1S_3)(L_3 - L_5) + C_1C_2(L_2 - g) \qquad (3)$$

$$P_y = (S_1C_2C_3 + C_1S_3)(L_3 - L_5) + S_1C_2(L_2 - g) \qquad (4)$$

$$P_z = S_2(L_2 - g) + S_2C_3(L_3 - L_5) \qquad (5)$$

where $S_i = \sin(\theta_i)$ and $C_i = \cos(\theta_i)$.

The closed form of inverse kinematics of the proposed arm is derived using the stan-

dard method [2], [11]. The joint angles for the given end-point position can be determined explicitly [1].

Hardware

The system hardware uses an IBM/AT microcomputer, which is hosting a four-node NCUBE parallel processor as the main controller of this robot. The parallel processor has four nodes and a PC/AT bus interface. Each node is an independent 32-bit processor with local memory and communication links to the other nodes in the system. A high-speed analog-to-digital/digital-to-analog (AD/DA) converter has been used for reading the velocity signals and sending analog command signals to the servo controller unit. A parallel input/output board between the servo controller unit and the computer allows for reading the resolver-to-digital (R/D) converter.

The servo controller unit produces three-phase, pulse-width-modulated (PWM), sinusoidal currents for the power amplifier. The servo controller unit contains an interpolator, R/D converter, and a communication interface for the computer. The servo controller unit can be operated in either a closed-loop velocity or current (torque) control mode (the current control is used). A PWM power amplifier, which provides up to 47 A of drive current from a 325-V power supply, is used to power the motors. The main DC bus power is derived by full-wave rectifying the three-phase 230-VAC incoming power. This yields a DC bus voltage of 325 VDC.

The actuators used in this robot are neodymium (NdFeB) magnet AC brushless synchronous motors. Due to the high magnetic field strength (maximum energy products: 35 MGOe) of the rare earth NdFeB magnets, the motors have a high torque-to-weight ratio. Pancake-type resolvers are used as position and velocity sensors. The peak torque of motor 1 is 118 Nm, whereas the peak torques of motors 2 and 3 are 78 and 58 Nm, respectively.

Experimental Results

We describe two sets of experiments herein. First, the performance of the robot is measured in unconstrained space as a tracking accuracy along a specified trajectory. Second, the stability of the robot in constrained maneuvers has been analyzed and verified experimentally. In constrained maneuvers, the contact forces must be accommodated rather than resisted [12]–[16].

A feedforward compensator, as shown in Fig. 4, is used to cancel the robot nonlinear

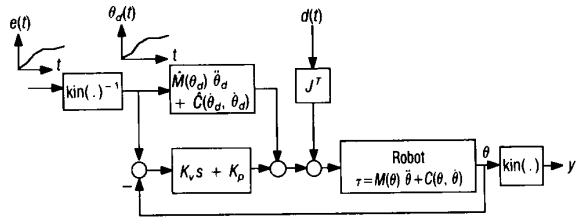

Fig. 4. Robot and feedforward torque controller dynamics.

terms, whereas a set of constant gains is used in the feedback loop to decrease the error and develop robustness in modeling errors. Because this robot does not contain any gearing, frictional losses are small and, consequently, the manipulator can be modeled using the Lagrangian approach [17], [18]. Trajectory control for the manipulator is performed by digital implementation of a feedforward torque controller, which is given by the following equation, where τ is the vector of joint torques; $(\theta_d - \theta)$ is the error between the command position, θ_d, and the actual position, θ; and $(\dot{\theta}_d - \dot{\theta})$ is the error between the respective velocities. K_p is a 3 × 3 diagonal matrix containing the position gains. K_v is a 3 × 3 diagonal matrix containing the velocity gains. $\hat{M}(\theta_d)$ is the estimated inertia matrix; $\hat{C}(\theta_d, \dot{\theta}_d)$ is the estimated 3 × 1 vector of centrifugal and Coriolis forces.

$$\tau = K_p(\theta_d - \theta) + K_v(\dot{\theta}_d - \dot{\theta}) + \hat{M}(\theta_d)\ddot{\theta}_d + \hat{C}(\theta_d, \dot{\theta}_d) \qquad (6)$$

The physical reasoning behind this control law is that the nonlinear feedforward terms, $\hat{M}(\theta_d)$ and $\hat{C}(\theta_d, \dot{\theta}_d)$, tend to cancel the effects of the nonlinear effects of $M(\theta)$ and $C(\theta, \dot{\theta})$ (inertia and Coriolis forces) in the robot's dynamics and result in a nearly uncoupled, linear system. The kin(.) operator in Fig. 4 represents the forward kinematics, whereas $\text{kin}^{-1}(.)$ represents the inverse kinematics. When the trajectory is specified in Cartesian space as a function of time, $e(t)$, the inverse kinematics and numerical differentiation are employed to transform it into joint space, $\theta_d(t)$.

All the joints were commanded to simultaneously move 30 deg in 0.3 sec on a cubic polynomial from a predetermined origin. The maximum velocity and acceleration for each joint are 150 deg/sec and 2000 deg/sec^2, respectively. The robot control program, written in C language, yields a 250-Hz sampling frequency. The trajectory error plots for each joint are depicted in Fig. 5, where the peak trajectory errors are 0.7, 1.2, and 0.44 deg for joints 1, 2, and 3, respectively.

Although feedforward torque control is computationally efficient, this method does

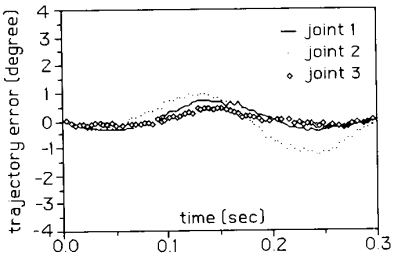

Fig. 5. Trajectory error; all the parameters are experimentally identified [1].

not achieve perfect uncoupling of each joint. Note that, despite the assumption that the robot dynamics are known accurately, the joints are not uncoupled perfectly; the degree of coupling varies as a function of the configuration.

The second set of experiments concerns the performance of the robot in constrained maneuvers. Figure 6 shows the system architecture when the robot interacts with the environment and when the robot compliancy is tailored by means of an H compensator. The H block is a part of the compliance controller and is implemented in the digital controller. The product of the environment mapping, E, is an external force, f, which is expressed in the global Cartesian coordinate frame. Although the trajectory controller operates in the manipulator joint space, H has been implemented as a linear transfer function, which can accept the Cartesian force and produce a Cartesian displacement. The product of H is a small displacement. In practice, $r(t)$ is transformed into joint space prior to execution; the inverse Jacobian, J^{-1}, is substituted for $\text{kin}^{-1}(.)$ in the system. The command $r(t)$ is used for both constrained and unconstrained maneuvers. When the robot is not in contact with the environment, $f = 0$ and the robot is driven by its tracking controller, $r(t)$. When the robot comes in contact with the environment, then the contact force follows the input command, $r(t)$.

To guarantee the stability of the system of Fig. 6, H must be chosen such that its "size" in the singular-value sense is smaller than

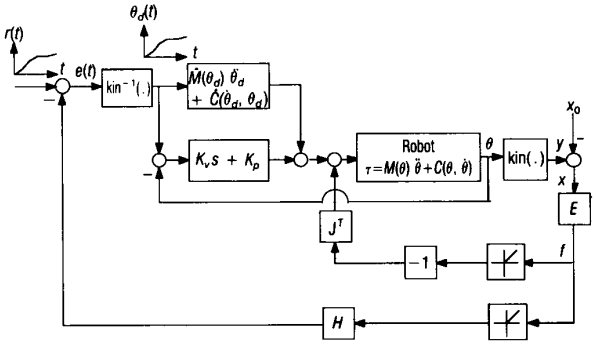

Fig. 6. Trajectory controller, robot dynamics, environment dynamics, and compliance compensator.

the size of the sensitivity of the robot [19]. We define the sensitivity of the robot in a global coordinate frame as a mapping from the imposed forces on the robot to the robot position. If the command $r(t)$ does not have any high-frequency components, the smallest value for the sensitivity function is $JK_p^{-1}J^T$. One must calculate the minimum singular value of $(JK_p^{-1}J^T)$ at each point in the commanded trajectory. The infimum is the lowest of all the minimum singular values. The gain of H (expressed in terms of its singular values) must be chosen smaller than this infimum. The stability region will approach zero when the robot maneuvers near a singular point [$\det(J) \rightarrow 0$] and/or when the position gains approach infinity. Both cases are instances of "infinite stiffness" for the robot; the first is due to the robot configuration, and the second is due to the tracking controller.

For a sufficient stability condition, if the condition is satisfied, the stability is guaranteed; however, if the condition is violated, no conclusion can be made. In the first experiment, we design an H such that the stability condition is satisfied and show, through experiment, that the system is stable. In the second experiment, we show that an H that destabilizes the system also violates the stability condition.

A reinforced aluminum wall was mounted vertically in the robot workspace. Motor 2 was mechanically locked, and motors 1 and 3 were used to actuate the robot for horizontal maneuvering; this resulted in planar, horizontal motion of the robot end point in global, Cartesian space. A force sensor is mounted on the manipulator end point to measure the contact forces. Since the experiments are all two-dimensional, H is a 2×2 matrix operating on contact forces that are normal and tangential to the wall. (The end-point force measurements were resolved into the global coordinate frame.) In these experiments, only the compliancy in the direction normal to the wall was supplemented, so the following form of H was chosen, where $T = 0.05$.

$$H = \begin{bmatrix} H_0/(Ts + 1) & 0 \\ 0 & 0 \end{bmatrix} \qquad (7)$$

The function $r(t)$, shown in Fig. 7 by the dashed line, is chosen as the assigned trajectory to the robot. Since H has only one nonzero member, then its maximum singular value will be the magnitude of $H_0/(Tj\omega + 1)$. The maximum of the maximum value of H is H_0 and occurs at DC ($\omega = 0$).

In the first experiment, we show that if stability is satisfied for a maneuver shown in Fig. 7, then the robot can interact with the environment stably. We choose H_0 to be 0.0003, so $H(s)$ was smaller than $\sigma_{\min}(JK_p^{-1}J^T)$ for all configurations within the maneuver. Figure 8 shows the experimental value of the normal contact force. The stable contact was indicated by the absence of undamped oscillations in the normal force.

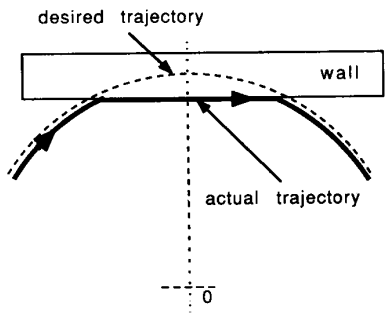

Fig. 7. Top view of experimental setup. The dashed line is the desired end-point trajectory, and the solid line is the actual trajectory.

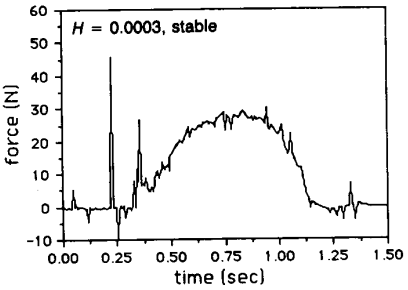

Fig. 8. Experimental measurement of the stable normal contact force. $H_0 = 0.0003$ satisfies the stability condition.

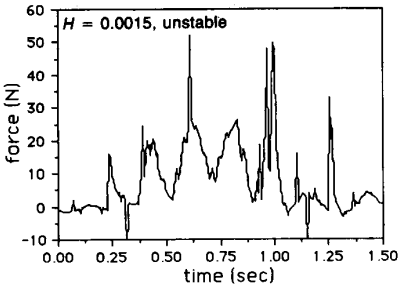

Fig. 9. Experimental measurement of the unstable normal contact force. $H_0 = 0.0015$ does not satisfy the stability condition.

In the second experiment, H_0 was set to 0.0015. Figure 9 shows the experimental value of the normal contact force as a function of time. In both results, the contact force oscillates throughout the maneuver, indicating that the compliance controller was unstable. The comparison with the singular-value plot shows that H_0 exceeded the lower bound on $\sigma_{\min}(JK_p^{-1}J^T)$; hence, the stability condition has been violated. Since the stability criterion is only a sufficient condition for stability, violation of this condition does not lead to any conclusion.

Summary

This paper presents some results of the ongoing research project on a statically balanced direct-drive arm at the University of Minnesota. The statically balanced mechanism without counterweights allows for selection of smaller actuators. Since in static or quasistatic operations there is no load on the actuators, the overheating of the previous direct-drive robots is alleviated. The robot links are made of graphite-epoxy composite materials to give more structural stiffness and less mass. The high structural stiffness and low mass of the links allow for the wide

bandwidth of the control system. To improve tracking errors, the robot parameters were identified experimentally. The errors in the trajectory and velocity were reduced significantly. Stability of the robot when it interacts with a hard environment has been derived and experimentally verified.

References

[1] H. Kazerooni and S. Kim, "A New Architecture for Direct Drive Robots," in *Proc. IEEE Intl. Conf. on Robotics and Automation*, Philadelphia, PA, vol. 2, pp. 1166–1172, Apr. 1988.

[2] J. J. Craig, *Introduction to Robotics: Mechanics and Control*, Reading, MA: Addison-Wesley, 1986.

[3] M. G. Forrest-Barlach and S. M. Babcock, "Inverse Dynamics Position Control of a Compliant Manipulator," *IEEE 1986 Intl. Conf. on Robotics and Automation*, vol. 1, pp. 196-205, Apr. 1986.

[4] E. I. Rivin, "Effective Rigidity of Robot Structures: Analysis and Enhancement," *Proc. 1985 Amer. Contr. Conf.*, Boston, MA, vol. 1, pp. 381–382, 1985.

[5] H. Asada and T. Kanade, "Design of Direct Drive Mechanical Arms," *ASME J. Vibration, Acoustics, Stress, and Reliability in Design*, vol. 105, no. 3, pp. 312–316, July 1983.

[6] H. Asada and H. Youcef-Toumi, "Analysis and Design of a Direct Drive Arm with a Five-Bar-Link Parallel Drive Mechanism," *ASME J. Dyn. Syst., Measurement, Contr.*, vol. 106, no. 3, pp. 225–230, 1984.

[7] K. Takase, T. Hasegawa, and T. Suehiro, "Design and Control of a Direct Drive Manipulator," *Proc. Intl. Symp. on Design and Synthesis*, Tokyo, Japan, pp. 333–338, July 1984.

[8] H. Kuwahara, Y. One, M. Nikaido, and T. Matsumoto, "A Precision Direct Drive Robot Arm," in *Proc. Amer. Contr. Conf.*, Boston, MA, vol. 2, pp. 722–727, 1985.

[9] S. Mahalingam and A. M. Sharan, "The Optimal Balancing of the Robotic Manipulators," *IEEE 1986 Intl. Conf. on Robotics and Automation*, San Francisco, CA, vol. 2, pp. 828-835, Apr. 1986.

[10] H. Kazerooni and P. K. Houpt, "On the Loop Transfer Recovery," *Intl. J. Contr.*, vol. 43, no. 3, pp. 981-996, 1986.

[11] R. P. Paul, *Robot Manipulators: Mathematics, Programming, and Control*, Cambridge, MA: MIT Press, 1981.

[12] N. Hogan, "Impedance Control, An Approach Manipulation," *ASME J. Dyn. Syst., Measurement, Contr.*, vol. 107, no. 1, pp. 1-24, Mar. 1985.

[13] H. Kazerooni, T. B. Sheridan, and P. K. Houpt, "Fundamentals of Robust Compliant Motion for Robot Manipulators," *IEEE J. Robotics and Automation*, vol. 2, no. 2, pp. 83-92, June 1986.

[14] H. Kazerooni, P. K. Houpt, and T. B. Sheridan, "Design Method for Robust Compliant Motion for Robot Manipulators," *IEEE J. Robotics and Automation*, vol. 2, no. 2, pp. 93-105, June 1986.

[15] H. Kazerooni and T. I. Tsay, "Stability Criteria for Robot Compliant Maneuvers," *Proc. IEEE Intl. Conf. on Robotics and Automation*, Philadelphia, PA, vol. 2, pp. 1166–1172, Apr. 1988.

[16] H. Kazerooni, "Direct-Drive Active Compliant End Effector (Active RCC)," *IEEE J. Robotics and Automation*, vol. 4, no. 3, pp. 324–333, June 1988.

[17] H. Asada and J-J. E. Slotine, *Robot Analysis and Control*, New York: Wiley, 1986.

[18] J. Y. S. Luh, M. W. Walker, and R. P. Paul, "Resolved—Acceleration Control of Mechanical Manipulators," *IEEE Trans. Autom. Contr.*, vol. AC-25, no. 3, pp. 468-474, June 1980.

[19] H. Kazerooni, S. Kim, and B. J. Waibel, "Theory and Experiments on the Robot Compliance Control," ASME Winter Annual Meeting on Robotics, Chicago, Dec. 1988.

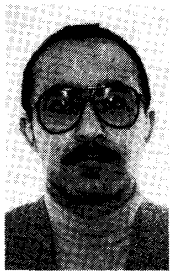

H. Kazerooni was born in Tehran, Iran, in May 1956. He received the M.S. degree in mechanical engineering from the University of Wisconsin, Madison, in 1980, and the M.S.M.E. and Sc.D. degrees in mechanical engineering from the Man-Machine Systems Laboratory of the Massachusetts Institute of Technology, Cambridge, in 1982 and 1984, respectively. From 1984 to 1985, he was with the Laboratory of Manufacturing and Productivity of the Massachusetts Institute of Technology as a Postdoctoral Fellow. He is currently Assistant Professor in the Mechanical Engineering Department at the University of Minnesota, Minneapolis.

ICCON '89

The International Conference on Control and Applications (ICCON) is a new conference sponsored by the IEEE Control Systems Society, and cosponsored and hosted by the IEEE Israel Section. The conference is to be held April 3-6, 1989, at the new Hyatt Regency Hotel in Jerusalem, Israel. The conference will provide an international forum for the presentation of technical papers that involve theory, design tools, and applications of control systems methods. Case studies are encouraged as an illustration of the methods and tools. Presentations will be made on computer-aided control system design tools and real-time computing for control systems. Professor Alexander Lerner has agreed to be a plenary speaker. The location, the most modern hotel in Israel, with beautiful scenery overlooking Jerusalem from Mt. Scopus, is meant to provide an excellent forum for informal discussions in addition to the formal paper presentations.

For further information, contact:
Cochairman: Yaakov Bar-Shalom, ESE Dept., University of Connecticut, Box U-157, Storrs, CT 06268 USA; phone: (203) 486-4823.
Program Chairman: Jürgen Ackermann, DFVLR, Oberpfaffenhofen, D-8031 Wessling, West Germany; phone: [49]-(8153)-281.
Program Vice Chairman—Invited Sessions: Michael Grimble, Dept. of Electrical Engineering, University of Strathclyde, Glasgow C1 1XW, Scotland, United Kingdom; phone: (44)-(41)-552-4400.

View of Jerusalem.